The Astrophysical Journal, 843:101 (8pp), 2017 July 10 https://doi.org/10.3847/1538-4357/aa799b

Double Arc Instability in the Solar Corona

N. Ishiguro and K. Kusano
Institute for Space-Earth Environmental Research, Nagoya University, Furo-cho, Chikusa-ku, Nagoya, Aichi 464-8601 Japan; n-ishiguro@isee.nagoya-u.ac.jp
Received 2016 October 12; revised 2017 June 12; accepted 2017 June 12; published 2017 July 11

Abstract

The stability of the magnetic field in the solar corona is important for understanding the causes of solar eruptions. Although various scenarios have been suggested to date, the tether-cutting reconnection scenario proposed by Moore et al. is one of the widely accepted models to explain the onset process of solar eruptions. Although the tether-cutting reconnection scenario proposes that the sigmoidal field formed by internal reconnection is the magnetic field in the pre-eruptive state, the stability of the sigmoidal field has not yet been investigated quantitatively. In this paper, in order to elucidate the stability problem of the pre-eruptive state, we developed a simple numerical analysis in which the sigmoidal field is modeled by a double arc electric current loop and its stability is analyzed. As a result, we found that the double arc loop is more easily destabilized than the axisymmetric torus, and it becomes unstable even if the external field does not decay with altitude, which is in contrast to the axisymmetric torus instability. This suggests that tether-cutting reconnection may well work as the onset mechanism of solar eruptions, and if so, the critical condition for eruption under a certain geometry may be determined by a new type of instability rather than by the torus instability. Based on them, we propose a new type of instability called double arc instability (DAI). We discuss the critical conditions for DAI and derive a new parameter κ, defined as the product of the magnetic twist and the normalized flux of the tether-cutting reconnection.

Key words: instabilities – Sun: corona – Sun: coronal mass ejections (CMEs) – Sun: filaments, prominences – Sun: flares

1. Introduction

The stability of the current-carrying magnetic flux rope is important for understanding the mechanism of solar eruptions, which are observed as flares, filament eruptions, and coronal mass ejections (CMEs). Various studies have tried to elucidate the stability and equilibrium conditions. Many theoretical models have been developed using the thin current model, e.g., the straight current loop model (Kuperus & Raadu 1974; van Tend 1979; Molodenskii & Filippov 1987; Forbes & Isenberg 1991), the axisymmetric current loop model (Chen 1989; Titov & Démoulin 1999; Kliem & Török 2006), and other shape models (Garren & Chen 1994; Isenberg & Forbes 2007; Olmedo et al. 2013) as reviewed by Aulanier (2014), in which the force acting on the thin electric current loop was calculated to analyze the stability, equilibrium conditions, or dynamics of the loop.

The axisymmetric torus instability (Shafranov 1966; Bateman 1978) was applied by Kliem & Török (2006) to explain the mechanism of solar eruptions using the thin current loop model. In that study, the flux rope was modeled by a half-circular torus of the electric current rooted on the solar surface. An image current is introduced into the subphotospheric region to satisfy the conditions on the solar surface; hence, the current channel effectively forms an axisymmetric torus. In this torus model, only the self-similar expansion of the torus can be allowed; therefore, the state variables are the radius R of the torus and the electric current I flowing on the torus. When an external magnetic field across the torus is imposed, the equilibrium in which the outward hoop force of the torus balances the inward force due to the external field can be satisfied by the condition $I = I_{\rm eq}(R)$.

The stability of the torus is determined by the sign of the force acting on the torus when R and I are displaced from the state of equilibrium under a constraint, such as the conservation of magnetic flux linking the torus. For instance, Kliem & Török (2006) found that when the external field is proportional to R^{-n}, the instability requires

$$n > n_{\rm crit} = \frac{3}{2} - \frac{1}{4c}, \tag{1}$$

where n is the decay index of the external magnetic field $\boldsymbol{B}_{\rm ex}$, which is defined by

$$n \equiv -\frac{\partial \ln |B_{\rm ex}|}{\partial \ln R}. \tag{2}$$

The coefficient c is given by $c = L/\mu_0 R$, where L is the inductance of the torus and μ_0 is the permeability of vacuum. This result indicates that when the decay index is larger than the critical index $n_{\rm crit}$, the force of the external field becomes weaker than the hoop force if the torus expands from equilibrium; hence, the torus becomes unstable in axisymmetric expansion. This is called the torus instability and corresponds to the axisymmetric torus mode of the ideal magnetohydrodynamic (MHD) instabilities in torus plasmas (Shafranov 1966; Bateman 1978). Démoulin & Aulanier (2010) demonstrated that the loss of equilibrium (LoE; compare Forbes & Isenberg 1991) and the criticality of torus instability occur at the same physical state. Kliem et al. (2014) also suggested that the fold catastrophe due to the LoE and torus instability is an equivalent description for the onset of solar eruptions. Although the models of axisymmetric torus instability allow the movement of footpoints across the solar surface, Isenberg & Forbes (2007) developed the expression for the line-tied equilibrium of a partial torus, based on the flux rope

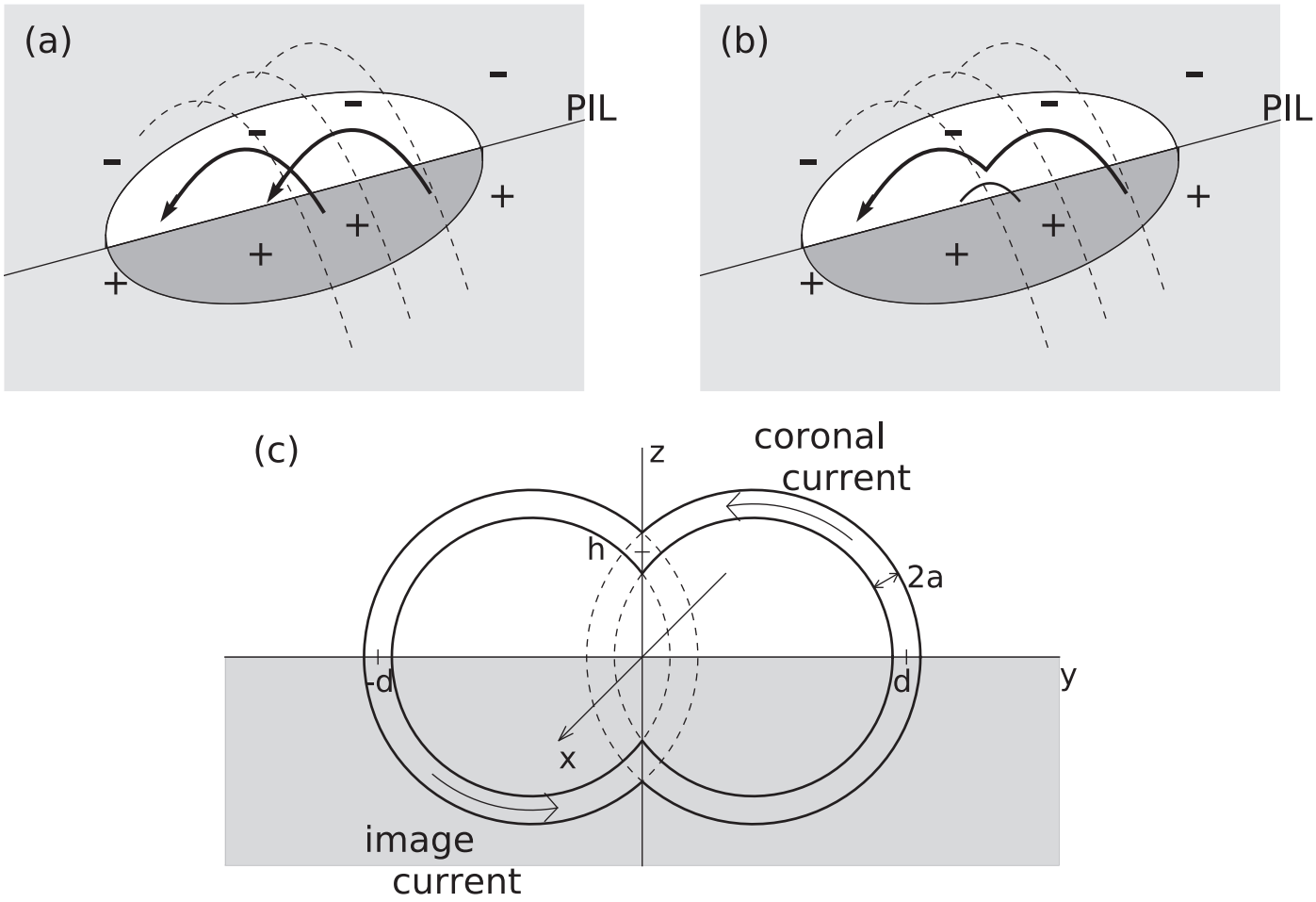

Figure 1. (a)(b) Illustration of tether-cutting reconnection in a strongly sheared polarity inversion line (PIL). The solid arrows are the current loops strong sheared initially. The dark gray (white) region is the positive (negative) polarity region. The dashed lines are the ambient potential magnetic field. (c) Schematic of the double arc electric current loop. Solid lines show the shape of the current loop, and the arrows denote the direction of the electric current. The thickness of the loop, $2a$, is uniform. The x-axis is orthogonal to the plane of the loop, that is, the y–z plane. The x–y plane corresponds to the solar surface (photosphere).

configuration of Titov & Démoulin (1999). Numerical studies confirmed that the torus instability can also occur in the case when the line-tied effect is included and not just in the case of a thin current channel (Fan & Gibson 2007; Török & Kliem 2007).

Although torus instability can well explain the growth of solar eruptions, the mechanisms causing the onset of solar eruption and initiating the instabilities are still unclear. Several possible scenarios have been proposed so far. The injection of magnetic helicity into the flux rope owing to photospheric twist motion possibly destabilizes the flux rope (Chen 1989), which was recently disproved by Schuck (2010). In addition, the decaying of the external field owing to the change of the photospheric magnetic field is another possible scenario to access the unstable state (Antiochos et al. 1999; Bobra et al. 2008). On the other hand, the tether-cutting reconnection scenario proposed by Moore et al. (2001) is one of the widely cited models to explain the formation of an unstable configuration of solar eruptions. The tether-cutting reconnection scenario explains that the eruption of the sigmoidal field formed by the internal reconnection between sheared field lines can play an important role in the initiation of eruptions. The "tether-cutting" scenario is consistent with the recent observations of Chen et al. (2014) and the numerical modeling of Kusano et al. (2012), who found that the pre-flare reconnection between the sheared arcade and the small-scale magnetic flux of typical orientations agrees with the tether-cutting scenario. The recent high-resolution observation with New Solar Telescope at Big Bear Observatory (Wang et al. 2017) indicates that the detailed evolution of pre-flare brightening is well consistent with the flare trigger model by Kusano et al. (2012).

Although it is likely that the instability of the sigmoidal magnetic field causes the onset of solar eruption, the stability of the sigmoidal field has not yet been investigated quantitatively due to the complexity of the field structure. The objective of this paper is to shed light on the stability of the sigmoidal field, which is formed by the internal reconnection between two sheared fields. In order to achieve it, we introduce a simple kinematic model, in which the sigmoid is modeled as a double arc shaped electric current loop, which is thought to be formed by tether-cutting reconnection, as illustrated in Figure 1(a). Through numerical analysis of the stability of the simple circuit model, we also aim to answer the question of what determines the critical state of stability of the sigmoidal magnetic field.

The paper is organized into the following sections. In Section 2, we explain the model for the double arc electric current loop and our numerical analysis. We will show the results of the calculations in Section 3, and discuss the critical

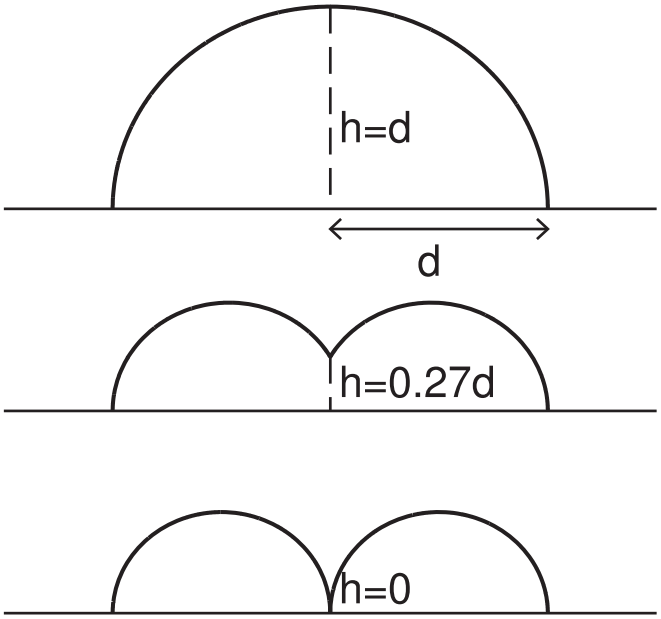

Figure 2. Examples of the double arc loop in the coronal region for $h = d$, $0.27d$, and 0. The footpoints of the loop are fixed to the solar surface, and this constraint corresponds to the line-tied condition. The geometry of the loop is parameterized by the joint height h.

parameter of the stability of the sigmoidal field based on the numerical analysis in Section 4. Finally, we summarize the conclusions in Section 5.

2. Model, Equations, and Numerical Analysis

2.1. Model

We model the sigmoidal field as a double arc electric current loop (Figure 1(b)), which can be formed by tether-cutting reconnection as illustrated in Figure 1(a). The double arc electric current loop is assumed to consist of two circles which are joined with each other at the center and rooted in the solar surface, as shown in Figure 1(c). To simplify the analysis, the double arc loop is assumed to be on the y–z plane, and the external field $\boldsymbol{B}_{\rm ex}$ on this plane is perpendicular to the plane. We also assume that the electric current I uniformly flows along the double arc and the radius of the cross-section, a, is small enough compared with the size of the arc. The roots of the loop and the joining point of the arcs are at $(y, z) = (\pm d, 0)$ and $(0, h)$, respectively. Since the roots of the arc are fixed, the state variables are only h and I, and the location of the roots d and the external field are fixed. The joint height h can vary only in the range from 0 to d, in which the double arc becomes a circle of radius d for $h = d$, as shown in Figure 2. It means that this model can be applied only in the early stage of eruption, and we cannot judge whether the sigmoid can fully erupt to CME with our model. This model cannot take into consideration the thickness of the loop and the change in loop shape from circular arc. These assumptions are introduced because we focus on the onset phase of eruption. The channel of electric current in the sigmoid may be thin and small at the very early stage of tether-cutting reconnection, although the sigmoidal field can develop into a thick and big flux rope after the onset of eruption.

In our model, the external magnetic field (dotted lines in Figures 1(a) and (b)) is assumed to be a potential field, and the effects of a magnetic field component pointing along the double arc loop is not taken into account. Because the tension force of a possible magnetic field component along the double arc loop and the Lorentz force due to possible additional electric currents outside the double arc loop, which are ignored in our study, may work more to destabilize the double arc, our study is only relevant to the sufficient condition for the instability of the double arc loop.

The image current below the solar surface is introduced to satisfy the boundary condition that the normal component of the magnetic field on the solar surface is fixed. Therefore, we analyze this stability of a figure-eight-shaped circuit subject to an external magnetic field.

2.2. Basic Equations

Although the current loop under consideration is not axisymmetric, we use the zero-dimensional model for the stability analysis, which is basically the same as that used by Démoulin & Aulanier (2010) for the torus instability. Here, the term of "zero-dimensional" means that the shape of the loop is constrained to be circles, which are characterized only by the parameter h, and the stability is analyzed by the variation of the total energy with respect to the displacement of h. First, we introduce the total magnetic field energy,

$$U = \frac{1}{2}L_{\rm tot}I^2 + I\Phi_{\rm ex}, \tag{3}$$

where $L_{\rm tot}$ is the total inductance given by the sum of the external inductance L_e and the internal inductance L_i of the current loop,

$$L_{\rm tot} = L_e + L_i, \tag{4}$$

and $\Phi_{\rm ex}$ is the magnetic flux through the area bounded by the double arc current loop and the solar surface. The generalized force F conjugate to the coordinate variable h is given by the derivative of U with respect to h (Shafranov 1966; Garren & Chen 1994), so that

$$F(h) = \frac{\delta U(h)}{\delta h} = \frac{1}{2}I^2\frac{\partial L_{\rm tot}(h)}{\partial h} + I\frac{\partial \Phi_{\rm ex}(h)}{\partial h}. \tag{5}$$

From the condition $F = 0$, we can obtain the equilibrium current,

$$I_{\rm eq}(h) = -2\frac{\partial \Phi_{\rm ex}(h)/\partial h}{\partial L_{\rm tot}(h)/\partial h} = -2\frac{\partial \Phi_{\rm ex}(h)}{\partial L_{\rm tot}(h)} \tag{6}$$

as a function of h. Here, note that the generalized force (Equation (5)) is not the force acting on each point on the electric current loop, but the net force, because it is derived from the variation of the total energy $U(h)$. So, the state corresponding to $F = 0$ is the equilibrium under the constraint that the loop is formed by the double arc, but is not the real equilibrium in which the force on any point should be zero. We will also discuss this limitation in Section 5.

If the loop evolves under the conditions of ideal MHD, in which any plasma motion is frozen in the magnetic field, the total magnetic flux through the area bounded by the double arc current loop and the solar surface must be conserved (Isenberg & Forbes 2007; Démoulin & Aulanier 2010). On the other hand, if magnetic reconnection proceeds below the erupting sigmoid, the magnetic flux across the loop can increase. In such

a case, because more flux is twisted around the core of the sigmoid, reconnection may work more to destabilize the system. Therefore, we adopt the constraint of ideal MHD to derive the sufficient condition for instability.

The total magnetic flux $\Phi_{\rm total}$ is described by the following equation.

$$\Phi_{\rm total} = L_e(h)I + \Phi_{\rm ex}(h). \tag{7}$$

From this equation, we can derive the evolutional current as a function of h,

$$I_{\rm evol}(h) = \frac{1}{L_e(h)}(\Phi_{\rm total} - \Phi_{\rm ex}(h)), \tag{8}$$

where the conserved flux $\Phi_{\rm total}$ is a parameter for determining the dynamical solution of h and I.

In this study, we analyze three different types of external fields, $\boldsymbol{B}_{\rm ex}^{(i)}$ for $i = 1$, 2, or 3. The first type of external field is the potential field given by the point sources of the magnetic flux ϕ located at $(x, y, z) = (\pm D, 0, 0)$, so that they make the following magnetic distribution on the $x = 0$ plane:

$$\boldsymbol{B}_{\rm ex}^{(1)}(\boldsymbol{x} = 0, \boldsymbol{y}, z) = \frac{-4D\phi}{(r^2 + D^2)^{3/2}}\frac{\boldsymbol{x}}{|\boldsymbol{x}|}, \tag{9}$$

where $r^2 = y^2 + z^2$. This field simulates sunspots of bipole type, as used in a previous study (Démoulin & Aulanier 2010). The second type of external field is the linear force-free field given by the boundary condition of the sinusoidal function of x, i.e., $B_z(x, y, 0) = B_0 \sin(x/L)$, where B_0 is a constant. The field on the $x = 0$ plane is given by

$$\boldsymbol{B}_{\rm ex}^{(2)}(\boldsymbol{x} = 0, \boldsymbol{y}, z) = -B_0 e^{-|z|/L}\frac{\boldsymbol{x}}{|\boldsymbol{x}|}. \tag{10}$$

The third type of external field is a uniform field:

$$\boldsymbol{B}_{\rm ex}^{(3)}(\boldsymbol{x} = 0, \boldsymbol{y}, z) = -B_0\frac{\boldsymbol{x}}{|\boldsymbol{x}|}. \tag{11}$$

This field corresponds to an extreme case in which the current loop is much smaller than the length scale L of the external field.

2.3. Numerical Analysis

Because of the structural complexity of the double arc loop, we use numerical analysis to derive the inductance L_e and magnetic flux $\Phi_{\rm ex}$, according to the expression by Garren & Chen (1994). The self-flux through the current loop is given by the line integral of the vector potential along the inner edge of the loop and the solar surface boundary,

$$\Phi = \oint \boldsymbol{A} \cdot d\boldsymbol{r}, \tag{12}$$

where the vector potential can be obtained by the volume integral of the current loop,

$$\boldsymbol{A} = \frac{\mu_0}{4\pi}\int \frac{I_0}{|\boldsymbol{r} - \boldsymbol{r}'|}d\boldsymbol{r}'. \tag{13}$$

Therefore, the external inductance L_e of the loop is calculated as

$$L_e = \Phi/I_0 = \frac{\mu_0}{4\pi}\oint\int \frac{1}{|\boldsymbol{r} - \boldsymbol{r}'|}d\boldsymbol{r}' \cdot d\boldsymbol{r}. \tag{14}$$

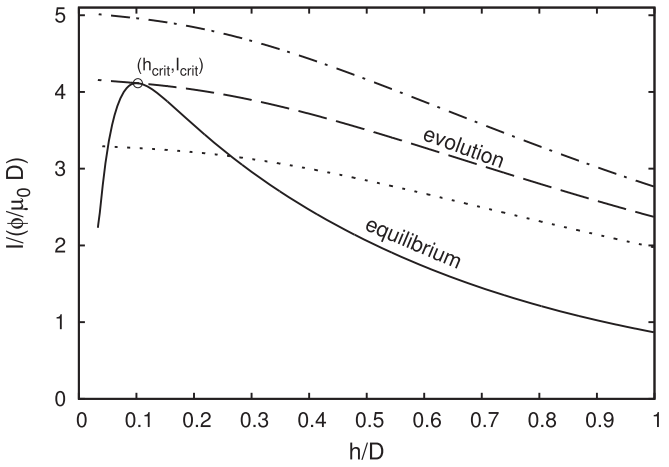

Figure 3. Relation between height h and electric current I. The horizontal axis is the normalized joint height h/D, and the vertical axis is the normalized electric current $I/(\phi/\mu_0 D)$. The solid line represents the equilibrium state, and the dotted, dashed, and dotted–dashed curves correspond to the states for $\Phi_{\rm total} = 0.7\Phi_0$, $1.0002\Phi_0$, and $1.3\Phi_0$, respectively. The circled mark is the critical point, which means that the right branch along the equilibrium curve is unstable and the left is stable.

The internal inductance L_i, which corresponds to the magnetic flux linked to the inner unit current of the loop, is

$$L_i = \frac{\mu_0 l_l}{8\pi}, \tag{15}$$

where l_l is the length of the loop. The external magnetic flux $\Phi_{\rm ex}$ is derived by the surface integral over the area bounded by the double arc current loop and the solar surface,

$$\Phi_{\rm ex} = \int \boldsymbol{B}_{\rm ex}^{(i)} \cdot d\boldsymbol{S} = \oint \boldsymbol{A}_{\rm ex}^{(i)} \cdot d\boldsymbol{r}. \tag{16}$$

For this line integration, we use the following vector potentials for the above-mentioned external fields $B_{\rm ex}$:

$$\boldsymbol{A}_{\rm ex}^{(1)}(\boldsymbol{x} = 0, \boldsymbol{y}, z) = \frac{2L\phi}{\sqrt{y^2 + z^2 + D^2}}\begin{pmatrix} 0 \\ \frac{z}{y^2 + D^2} \\ -\frac{y}{z^2 + D^2} \end{pmatrix}, \tag{17}$$

$$\boldsymbol{A}_{\rm ex}^{(2)}(\boldsymbol{x} = 0, \boldsymbol{y}, z) = -B_0 L\frac{z}{|z|}e^{-|z|/L}\frac{\boldsymbol{y}}{|\boldsymbol{y}|}, \tag{18}$$

$$\boldsymbol{A}_{\rm ex}^{(3)}(\boldsymbol{x} = 0, \boldsymbol{y}, z) = -B_0 y\frac{\boldsymbol{z}}{|z|}. \tag{19}$$

We use the second-order central difference to calculate the first-order derivative of Equation (6) and the trapezoidal integration. The loop is discretized into 16,000 grids along its length and 10 × 30 grids on a cross-section (radius × azimuth) of the loop.

We evaluate the numerical method by comparing the numerical solution of the axisymmetric torus instability with the analytical solution by Démoulin & Aulanier (2010) and confirm that the numerical results are consistent with the analytical results for a thin loop, $a \ll d$. Actually, in this study we focus only on the case of a thin loop in which $a/d = 10^{-3}$.

3. Results

In Figure 3, the results for the equilibrium current $I_{\rm eq}$ (solid line) and the evolutional current $I_{\rm evol}$ (dotted, dashed, and

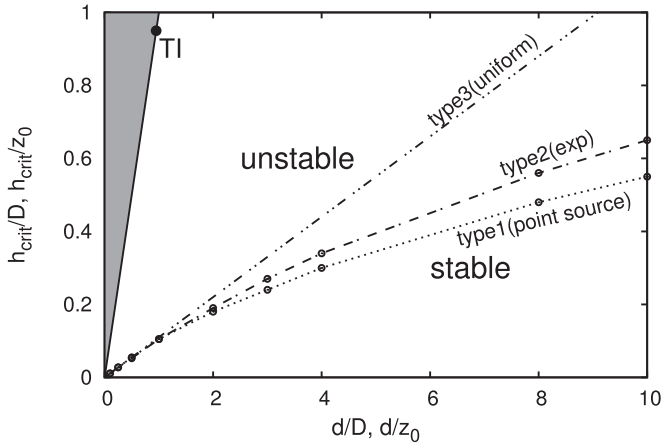

Figure 4. Critical height h_{crit} for types 1–3 external fields as a function of the half interval length between footpoints d, which are normalized by D (type 1) or L (type 2). The dashed–dotted, double-dashed–dotted, and dashed–double-dotted lines correspond to types 1, 2, and 3, respectively. The hatched region is outside the domain defined in the current model $0 \leqslant h \leqslant d$. The solid circle marked TI denotes the critical height above which axisymmetric torus instability can grow for type 1 external field.

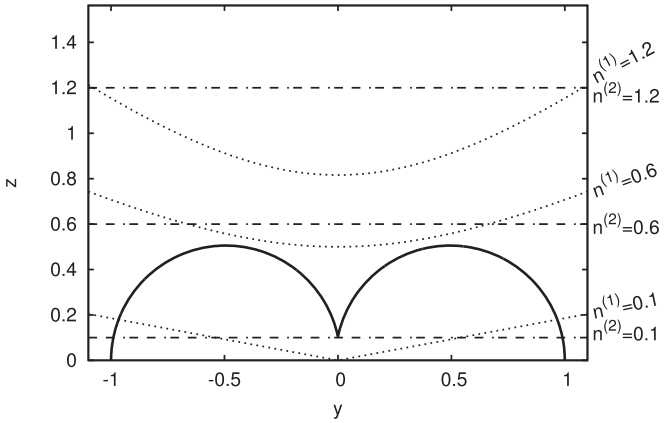

Figure 5. Contour map of the decay index for types 1 and 2 on the y–z plane. Here, the y and z axes are normalized by D or L, respectively. The dashed lines are the contours for $n^{(1)}$ and $n^{(2)} = 0.1$, 0.6, and 1.2. The solid line shows the double arc loop for $d = 1$ and $h = 0.105$.

dotted–dashed lines) are plotted as a function of h for the first type of external field $\boldsymbol{B}_{ex}^{(1)}$. The loop below the equilibrium curve moves downward owing to the downward force and is uplifted by the upward force in the region above the equilibrium curve. The equilibrium curve has a single peak at $P(h_p, I_p)$, and we define $\Phi_0 = \Phi_{total}(h_p, I_p)$. Three evolutional curves are plotted for $\Phi_{total} = 0.7\Phi_0$, $1.0002\Phi_0$, and $1.3\Phi_0$. The dashed evolutional curve for $\Phi_{total} = 1.0002\Phi_0$ is tangent to the equilibrium curve at the point (h_{crit}, I_{crit}), where $h_{crit}/D \simeq 0.105$. The critical point (h_{crit}, I_{crit}) corresponds to the LoE state, above which there is no equilibrium, and the left and right branches of the equilibrium curve from (h_{crit}, I_{crit}) are stable and unstable, respectively.

We calculate the critical height h_{crit} of the LoE state for types 2 and 3 of the external fields using the same method and plot the normalized results as a function of d in Figure 4.

From Figure 4, we find that h_{crit} increases with d in any external field. The results for types 1 and 2 are very similar. We emphasize that the critical height h_{crit} exists even in the case of a uniform external field (type 3). The critical height h_{crit} for type 3 is proportional to d because there is no characteristic scale in the external field, and its value is much smaller than d, i.e., $h_{crit} = 0.105d$. This suggests that the double arc current loop can be unstable even in the case where the external field does not decay with altitude.

This result is remarkably different from the result of axisymmetric torus instability. The axisymmetric loop becomes unstable if and only if the external field decays with the altitude more quickly than a certain rate. The condition for torus instability is satisfied when the loop height h and d are larger than $0.95D$ for a type 1 external field (corresponding to the solid circle TI in Figure 4). The critical height of the double arc loop is much lower than that of the axisymmetric loop when the external field decays (types 1 and 2). This result is consistent with the fact that h_{crit} for types 1 and 2 asymptotically converges to that of type 3 as d tends to zero because the external field in all cases is almost uniform near the bottom surface. Therefore, we can conclude that the double arc loop can be more easily destabilized than the axisymmetric loop and that it can become unstable even if the external field does not decay with altitude. Hereafter, we refer to the instability of the double arc loop as "double arc instability (DAI)."

The decay index, which is often referred to in the threshold of torus instability, is defined by

$$n = -\frac{z}{|B_{ex}|}\frac{\partial |B_{ex}|}{\partial z}. \tag{20}$$

The decay index for types 1–3 external fields is given by

$$n^{(1)} = \frac{3z^2}{y^2 + z^2 + D^2}, \tag{21}$$

$$n^{(2)} = \frac{|z|}{L}, \tag{22}$$

$$n^{(3)} = 0. \tag{23}$$

Figure 5 shows the contour map of $n^{(1)}$ and $n^{(2)}$. The solid curve denotes the double arc loop of the critical state for $d/D = 1$ and $h/D = h_{crit}/D$ for the type 1 external field. It is clear that the decay index on the loop is below about 0.6, which is similar to that in the case of the type 2 external field. In contrast, the decay index is zero everywhere in the case of the type 3 external field. All the results differ from those of the axisymmetric torus instability, in which the critical decay index is approximately 1.5 for the type 1 external field (Kliem & Török 2006; Démoulin & Aulanier 2010), and it cannot be unstable in a uniform external field (type 3). This means that the decay index is not a relevant index for the threshold of instability for the double arc loop.

4. Discussion

In the previous section, we showed that the instability of the double arc loop can grow even though the torus instability is stable. In this section, we discuss the conditions for DAI according to the tether-cutting reconnection scenario and also the dynamical processes after the onset of instability.

4.1. Critical Condition

The tether-cutting scenario proposes that the internal reconnection proceeds in the core of the sheared magnetic field in the pre-eruptive phase, and it may form a double arc flux rope (sigmoidal field) that carries an electric current I. Let us assume that the tether-cutting reconnection proceeds at a

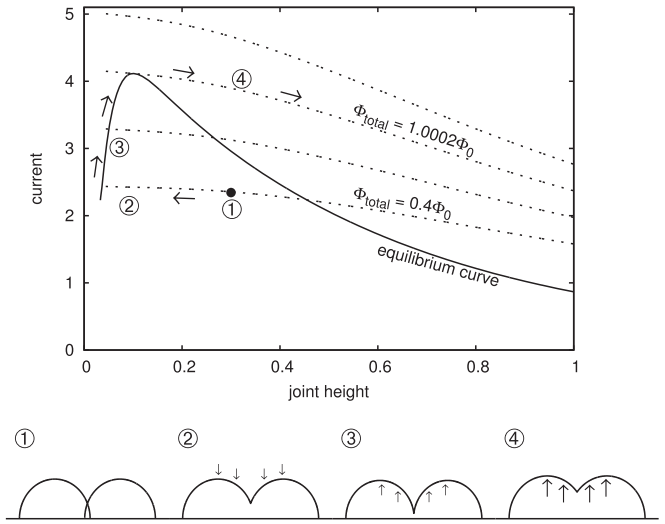

Figure 6. Dynamical process of the tether-cutting scenario on the parameter space of the electric current and joint height of the double arc. The upper diagram is the same as in Figure 3, in which each phase from the tether-cutting reconnection to the onset of eruption, ① to ④, is specified. The lower diagrams show the typical shapes and variations of the double arc in each phase.

certain height and forms a double arc loop denoted by the solid circle (phase ①) in Figure 6. If the height of the tether-cutting reconnection is below the equilibrium curve as in Figure 6, the joint height moves down along the evolutional curve and reaches the equilibrium state (phase ②). As reconnection proceeds further, the current I increases and the state variable gradually moves up along the stable branch of the equilibrium curve in Figure 6 (phase ③). Finally, the loop loses equilibrium and erupts when it overcomes the LoE point ($h_{\rm crit}$, $I_{\rm crit}$) (phase ④). Therefore, DAI may control the onset of eruption in the tether-cutting scenario.

Furthermore, we can discuss the critical condition for DAI caused by the tether-cutting reconnection based on the result of Figure 6. Let us assume that the pre-eruptive state is approximated by the force-free field, which is represented by the force-free equation $\nabla \times \boldsymbol{B} = \alpha \boldsymbol{B}$ with the force-free parameter α. Because the electric current density $\boldsymbol{J} = \nabla \times \boldsymbol{B}/\mu_0$ is proportional to $\boldsymbol{B}$ in the force-free field, if the magnetic flux $\Phi_{\rm rec}$ reconnects, the current flowing on the double arc loop is proportional to $\Phi_{\rm rec}$, i.e.,

$$I = \frac{\alpha}{\mu_0}\Phi_{\rm rec}. \tag{24}$$

According to the results of the numerical analysis in Figure 3, DAI grows when the electric current I is larger than the critical current $I_{\rm crit} \simeq 4\phi/\mu_0 d$ for a type 1 external field for $D = d$. This condition ($I > I_{\rm crit}$) corresponds to

$$\alpha d > \frac{4\phi}{\Phi_{\rm rec}}, \tag{25}$$

owing to the relation of the force-free field (24).

On the other hand, the twist of the magnetic field line is defined by $T = \int \alpha dl/4\pi$, where the integration is performed along the field line from one footpoint to the other. Because the force-free parameter α is constant along each field line, the twist of the single arc of diameter d is given by

$$T_0 = \frac{1}{4\pi}\pi\frac{d}{2}\alpha = \frac{\alpha d}{8}. \tag{26}$$

If we assume that tether-cutting reconnection occurs near the footpoint of the field lines of the force-free parameter α, then the twist of the double arc is approximated by

$$T \sim 2T_0 = \frac{\alpha d}{4}. \tag{27}$$

Using this relation and the total magnetic flux of the type 1 external field $\Phi_{\rm total} = 4\pi\phi$, we define a new parameter

$$\kappa = T\frac{\Phi_{\rm rec}}{\Phi_{\rm total}}. \tag{28}$$

Then, the condition for instability (25) is rewritten as follows:

$$\kappa > \frac{1}{4\pi} \tag{29}$$

for the external field of type 1.

In the case of type 2 external field for $L = d$, the critical electric current is given by

$$I_{\rm crit} \simeq \frac{B_0 d}{\mu_0}. \tag{30}$$

If we define the total magnetic flux as $\Phi_{\rm total} = \int_0^\infty dz \int_0^{2d} dy |B_{\rm ex}^{(2)}| = 2dLB_0$, the critical condition $I > I_{\rm crit}$ is written by

$$\kappa > \frac{1}{8}. \tag{31}$$

Also, in the case of type 3 external field, the critical electric current is $I_{\rm crit} \simeq 7B_0 d/5\mu_0$, and if we define the total flux as $\Phi_{\rm total} = 2d^2 B_0$, the critical condition is

$$\kappa > \frac{7}{40}. \tag{32}$$

The results above suggest that the critical condition for DAI is in general given by the condition

$$\kappa > \kappa_0, \tag{33}$$

in which the threshold κ_0 depends on the configuration of the external magnetic field. Because κ consists of the magnetic twist and the normalized reconnected flux, the critical condition (33) indicates that the magnetic twist and the tether-cutting reconnection play complementary roles in destabilizing DAI. If the twist is high enough, even a small amount of tether-cutting reconnection may trigger DAI, whereas more reconnection is required in a region of weaker twist.

This result is consistent with the analysis of Inoue et al. (2011), who investigated the twist and connectivity of the magnetic field of the active region NOAA 10930 using vector magnetograms obtained by the Solar Optical Telescope onboard the *Hinode* spacecraft and nonlinear force-free field extrapolation. They showed that the magnetic flux in the flaring region was twisted by more than a half turn one day prior to the onset of flares. If we apply the critical condition (29) to this active region, since the magnetic twist of the field lines prior to tether-cutting reconnection, T_0, is approximated to be $1/2$, the required flux for the tether-cutting reconnection for

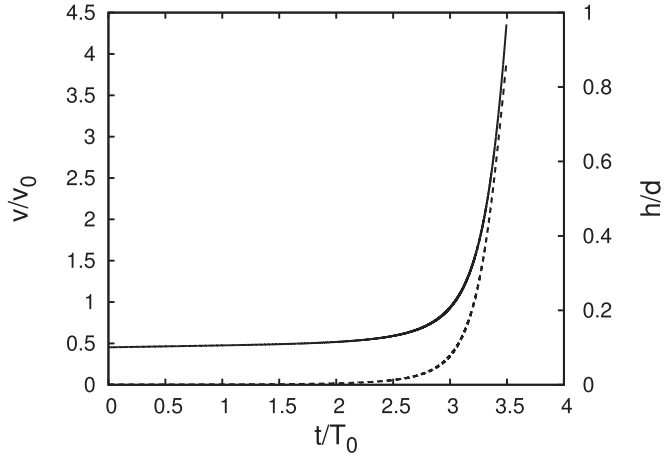

Figure 7. Temporal evolution of the DAI for velocity v (dotted curve) and height of joint point h (solid curve) for the type 1 external field. The time t is normalized by the Alfvén time T_0, and the initial perturbation $\delta v/v_0 = 0.005$.

destabilizing DAI is about $\Phi_{\rm total}/4\pi$. Bamba et al. (2013) analyzed the magnetic field of this active region using the data measured by the *Hinode* satellite and found that the magnetic island, which may work to trigger the X3.4 flare at 02:14 UT, 2006 December 13, quickly grew before the onset of the flare. Although what fraction of the magnetic island was involved in the tether-cutting reconnection is not clear, because the area of the magnetic island was as wide as 10% of the major spot prior to the onset of the flare, the results are consistent with the critical condition for DAI.

Bamba et al. (2013) also pointed out that another X-class (X1.5) flare occurred at 22:07 UT on 2006 December 14 in the same active region, and the size of the magnetic island that triggered the event is much smaller than the X-class flare on December 13. The condition for DAI (33) may provide a possible explanation for how the difference in the critical size of the magnetic island between the two events might be due to the difference in magnetic twist before the two events, although we need more investigations to confirm this hypothesis.

The numbers $\kappa_0 \simeq 0.1$–0.2 obtained from Equations (29) to (32) also correspond nicely to the analysis with the flux rope insertion method in Su et al. (2011), Savcheva et al. (2012), and other studies by their group in 2008–2012. Without the outlier in Figure 8 in Savcheva et al. (2012), they calculated the range of the flux ratio thresholds, $\Phi_{\rm axi}/\Phi_{\rm tot} \simeq 0.1$–$0.3$. Their results are favorable for the thresholds of κ if we assume that the magnetic twist is in the range $T \simeq 0.5$–1.0 and the magnitude of $\Phi_{\rm axi}$ corresponds to that of $\Phi_{\rm rec}$.

4.2. Eruptive Dynamics of the DAI

Finally, we would like to discuss the dynamics of the instability under the constraint that the total flux across the double arc loop is conserved. This corresponds to phase ④ in Figure 6. Because the generalized force acting on the double arc loop is given by Equation (5), the velocity of the joint height $v = dh/dt$ is governed by the equation of motion,

$$m\frac{dv}{dt} = \frac{1}{2}I^2(h)\frac{\partial L_{\rm tot}(h)}{\partial h} + I(h)\frac{\partial \Phi_{\rm ex}(h)}{\partial h}, \qquad (34)$$

where m is the mass of the loop.

We solve Equation (34) for the critical state by imposing small perturbations. Figure 7 shows the result of the time evolution of the velocity (dotted curve) and joint height (solid curve) of the loop. The joint height h, velocity v, and time t are normalized by d, the Alfvén speed $v_0 = \phi d^{-2}(\rho\mu_0)^{-1/2}$, where ρ is the mass density, and the Alfvén time $T_0 = d/v_0$, respectively. The result clearly suggests that while the joint height of the loop slowly increases in the early phase before $t/T_0 = 2.5$, it quickly erupts afterwards. The velocity rapidly increases up to $4v_0$, when the joint height h approaches d.

For typical values of the solar corona of $d \simeq 40$ Mm, $\rho \simeq 0.5 \times 10^{-9}$ kg m^{-3}, and $B_0 \simeq 20$ G, the factors for normalization are $T_0 \simeq 500$ s and $v_0 \simeq 80$ km s^{-1}. Therefore, the results suggest that the current loop may accelerate to approximately 320 km s^{-1}, when the loop becomes an axisymmetric torus after the slow-rise phase of about 1200 s. This result is in good agreement with the observations of previous studies (e.g., Chifor et al. 2006), which show that the filament accelerated to more than 300 km s^{-1} in about 10 minutes.

5. Summary

We numerically analyzed the stability of the double arc electric current loop, which may form as a consequence of tether-cutting reconnection, and found a new type of instability called DAI. Our study suggests that while the critical height of the torus instability depends on the decay index of the external magnetic field (Kliem & Török 2006; Démoulin & Aulanier 2010), the critical condition for DAI is insensitive to the decay index. This is attributed to the fact that DAI is mainly caused by the variation of the inductance (the first term on the right-hand side of Equation (5)), whereas the torus instability is mainly caused by the variation of the external flux (the second term of Equation (5)). Therefore, the double arc loop can be unstable even in a uniform external field. This means that the decay index is not an adequate criterion for the onset of eruption if DAI is responsible for the early phase of solar eruption. These results reaffirm that the tether-cutting reconnection can efficiently work as the onset mechanism of eruptive events in the solar corona.

Our study clearly shows that the double arc loop can become unstable irrespective of the decay index, and the unstable double arc loop may obtain substantial kinetic energy when it grows to form an axisymmetric torus. Although our model can be applied only to the phase before the double arc loop becomes a torus, it is likely that DAI can play an important role in acceleration in the early phase of eruption. If the double arc loop cannot obtain enough kinetic energy after the growth of the DAI and if the loop cannot reach the region where the decay index does not exceed the critical threshold of the torus instability, the confined eruption will occur. In other words, however, we cannot judge whether the loop will expand to a CME or not only from our model of the DAI, because it depends on the interaction of the ejected loop with the magnetic field and plasma in the higher region. Thus, in order to forecast the formation of a CME, we have to construct a more generalized model; for instance, by connecting our model to that of the line-tied equilibrium developed by Isenberg & Forbes (2007).

Our model is a simple circuit model that cannot describe the rigorous shape of the double arc loop because we do not consider the dynamics of each segment in the loop. In particular, it is likely that the cusp shape of the magnetic field line at the tether-cutting reconnection point is quickly relaxed to a smoother concave shape just after reconnection, while the shape of each loop is restricted to a circle in our model. How the changes in the shape of the double arc loop affect its

stability remain to be solved. Therefore, we need to develop a more sophisticated numerical simulation based on the MHD equations to verify the dynamics of the DAI. The development of this type of simulation is currently in progress. Despite the multiple limitations of our model, the dynamical property of the DAI is well consistent with the previous observations and simulations, and we derived the critical condition for DAI, which can be described by the new parameter κ. Although further study is needed to verify the detailed properties of the DAI, it is likely that the DAI and its critical condition may provide a clue to understanding the onset problem of solar eruptions under a specific geometry.

We wish to thank B. Kliem, S. Imada, S. Inoue, D. Shyukuya, and T. Shibayama for their helpful comments and discussions. We are grateful to the referee for variable comments that improved the paper. This work was supported by JSPS/MEXT KAKENHI grant Nos. JP23340045 and JP15H05814. This study was carried out by using the computational resources of the Center for Integrated Data Science, Institute for Space-Earth Environmental Research, Nagoya University through the joint research program.

References

Antiochos, S. K., DeVore, C. R., & Klimchuk, J. A. 1999, ApJ, 510, 485
Aulanier, G. 2014, in IAU Symp. 300, Nature of Prominences and their Role in Space Weather, ed. B. Schmieder, J.-M. Malherbe, & S. T. Wu (Cambridge: Cambridge Univ. Press), 184
Bamba, Y., Kusano, K., Yamamoto, T. T., & Okamoto, T. J. 2013, ApJ, 778, 48
Bateman, G. 1978, MHD Instabilities (Cambridge, MA: MIT Press)
Bobra, M. G., van Ballegooijen, A. A., & DeLuca, E. E. 2008, ApJ, 672, 1209
Chen, H., Zhang, J., Cheng, X., et al. 2014, ApJL, 797, L15
Chen, J. 1989, ApJ, 338, 453
Chifor, C., Mason, H. E., Tripathi, D., Isobe, H., & Asai, A. 2006, A&A, 458, 965
Démoulin, P., & Aulanier, G. 2010, ApJ, 718, 1388
Fan, Y., & Gibson, S. E. 2007, ApJ, 668, 1232
Forbes, T. G., & Isenberg, P. A. 1991, ApJ, 373, 294
Garren, D. A., & Chen, J. 1994, PhPl, 1, 3425
Inoue, S., Kusano, K., Magara, T., Shiota, D., & Yamamoto, T. T. 2011, ApJ, 738, 161
Isenberg, P. A., & Forbes, T. G. 2007, ApJ, 670, 1453
Kliem, B., Lin, J., Forbes, T. G., Priest, E. R., & Török, T. 2014, ApJ, 789, 46
Kliem, B., & Török, T. 2006, PhRvL, 96, 255002
Kuperus, M., & Raadu, M. A. 1974, A&A, 31, 189
Kusano, K., Bamba, Y., Yamamoto, T. T., et al. 2012, ApJ, 760, 31
Molodenskii, M. M., & Filippov, B. P. 1987, SvA, 31, 564
Moore, R. L., Sterling, A. C., Hudson, H. S., & Lemen, J. R. 2001, ApJ, 552, 833
Olmedo, O., Zhang, J., & Kunkel, V. 2013, ApJ, 771, 125
Savcheva, A. S., Green, L. M., van Ballegooijen, A. A., & DeLuca, E. E. 2012, ApJ, 759, 105
Schuck, P. W. 2010, ApJ, 714, 68
Shafranov, V. D. 1966, RvPP, 2, 103
Su, Y., Surges, V., van Ballegooijen, A., DeLuca, E., & Golub, L. 2011, ApJ, 734, 53
Titov, V. S., & Démoulin, P. 1999, A&A, 351, 707
Török, T., & Kliem, B. 2007, AN, 328, 743
van Tend, W. 1979, SoPh, 61, 89
Wang, H., Liu, C., Ahn, K., et al. 2017, NatAs, 1, 0085